



Luminescence Study of nano $\text{BaMgAl}_{10}\text{O}_{17}:\text{Eu}^{2+}$ phosphor

A S Sai Prasad ¹and K. V. R. Murthy

Department of Physics

¹Vasavi College of Engineering (Autonomous),
Hyderabad, T.S. India

Display Materials Laboratory

Applied Physics Department,

Faculty of Technology and Engineering,

The M. S. University of Baroda, Vadodara – 390001 India

Corresponding author: drmurthykvr@yahoo.com:

H/P0091 9327225568

Abstract

Over the last few decades, intense research activities have been concentrated on rare earth and transition metal ion activated alkaline earth aluminate phosphors because they are widely used in a variety of applications, such as lamp industry, cathode ray tubes, projection televisions, color display and X-ray imaging. Hexagonal alkaline earth aluminate phosphors are typically produced by the solid-state reaction method. Combustion synthesis is a novel technique that has been applied to phosphor synthesis in the past few years. BAM host crystallizes as β -alumina structure. This indicates that the BAM has a layered structure with the stacking sequence of conduction planes and spinel block. In such a structure, it is possible to incorporate a large variety of divalent, rare earth and trivalent ions into the conduction plane and the spinel block. In this paper Eu doped $\text{BaMgAl}_{10}\text{O}_{17}$ phosphor was synthesized by combustion method. Phase analysis of prepared phosphor was done by (XRD model D2 PHASER, Bruker AXS) using $\text{Cu}/\text{K}\alpha$ radiation ($\lambda = 1.54060 \text{ \AA}$). Photoluminescence of $\text{BaMgAl}_{10}\text{O}_{17}$ phosphor have been investigated.

Experimental:

All the Europium doped phosphors are synthesized by solid state diffusion reaction method at high temperature. First the high purity materials of host, activators and the fluxes are blended, mixed and then fired at 1300°C for four hours in an alumina crucible covered with a lid in nitrogen atmosphere to get $2+$ state of the rare earth dopant. The product obtained is in the form of a cake formed because of firing and sintering. Then the cake is crushed and ball milled and then sorted to remove coarse and excessively crushed particles. The PL spectra were recorded at room temperature using the Shimadzu RF-5301 PC Spectrofluorophotometer. To get the nano material the received cake is ball milled for 12, 18, 24 and 36 hours. As per the standards of the ball mill it is assumed the sizes of the materials as follows: 12 hours 600nm, 18 hours 400nm, 24 hours 100nm and 36 hours 60nm.

2.2 Measurement:

The phase identification was carried out by powder X-ray diffraction at room temperatures, using a Bruker D2 Phaser, equipped with a vertical goniometer and $\text{CuK}\alpha$ radiation source of wavelength 1.54 \AA . The observation of morphology was carried out using Transmission Electron Microscopy (TEM), while a gross morphological description was obtained by Scanning Electron Microscopy (SEM) using a JEOL JSM-58 Scanning Microscope. Samples for TEM were

deposited onto 300 mesh copper TEM grids coated with 50 nm carbon films. Nanocrystalline samples dispersed in acetone were placed on the grid drop-wise. The excess liquid was allowed to evaporate in air. The grids were examined in JEOL 2010 microscope with Ultra-High Resolution (UHR) pole-piece using a LaB₆ filament operated at 200 kV. The photoluminescence excitation and emission were investigated using a Perkin-Elmer Luminescence Spectrometer (LS55B) at room temperature. For lifetime measurement of the doped Eu³⁺ ions, the multi-channel scaling (MCS) set up was used.

Results and Discussion

The crystal structure of the products was identified by X-ray diffraction analysis. Fig. 1 shows the typical XRD pattern of BAM:Eu²⁺ (nanosphere) is presented in figure 1. . All the reflections can be distinctly indexed to the pure monoclinic phase (space group P2₁/n). The XRD of nanorods, however, shows features that differ from the other morphologies in the range of $2\theta = (40^\circ - 55^\circ)$. This phenomenon is attributed to improved shape anisotropy in the nanorods. Lattice parameters of nanorod, nanosphere and bulk samples have been determined by 'TOPAZ' Software and have been tabulated in Table I. It is interesting to notice that the lattice parameters have been found to increase in nanorods and nanospheres with respect to the bulk sample.

The morphology and microstructure of synthesized BAM:Eu²⁺ nanospheres were further investigated by HRSEM presented in fig.2. The average width of the BAM:Eu²⁺ nanospheres, the mean diameter was 212.3 nm. The high resolution transmission electron micrograph (HRSEM) images [Figs 2] show the highly crystalline nature of BAM:Eu²⁺ nanospheres, with excellent phase purity.

While hydrothermal methods have been shown to be extremely effective in the synthesis of nanorods, nanotubes and nanowires, a unified theory is yet to emerge for the formation mechanisms of such structures. Based on relevant literature, three kinds of mechanisms - vapor-liquid-solid (VLS) growth, solution-liquid-solid (SLS) growth, and template-mediated processes have been proposed for the formation of crystalline 1D nanostructures. However, the formation of the nanorods in our synthetic system would not be dominated by the above-mentioned three processes. We deliberately avoided the application of external additives such as surfactants, polymers or strong chelating ligands, which would have had a profound effect on the growth mechanism, either by serving as energetically favorable sites for absorption of reactant molecules (VLS process), or by acting as a template to guide the directional growth of nanowires (template-confined synthesis). Thus, it can be concluded that the morphology evolution of BAM:Eu²⁺ is closely related to its inherent crystal structure. The monoclinic structure adopted by BAM:Eu²⁺ has been demonstrated to be highly anisotropic, facilitating the formation of various 1D nanostructures in template-free solution environments.

Previously, Peng *et al.* have investigated the effect of chemical potential on the shape evolution of CdSe nanocrystals with Wurtzite structure, and it has been observed that elevated chemical potential values of a species, generated by high monomer concentrations in the growth solution, leads to the formation of elongated structures. Li *et al.* found that a higher chemical potential was a dominant driving force for the growth of hexagonal lanthanide hydroxide nanowires during hydrothermal treatment. In the present case, the growth mechanism has been explained with the help of a similar scenario, where chemical potential of a species determines its aggregation kinetics and geometry. According to Peng's theory, when the concentration of

monomer in the bulk solution is high, the chemical potential of the monomer species in the bulk solution is considerably higher than that in the stagnant solution in direct contact with any facet of the growing crystal. As a result of such a concentration gradient, there is monomer diffusion, and the unique structural features of the particular ‘long axis’ facets direct the growth in a specific direction. The reactivity of different facets plays a vital role in this 1D growth process. After a certain interval of time, a situation arises when the chemical potential of the monomer in the bulk solution drops to a value lower than the chemical potential of the two unique facets, but remains higher than that of the others. Under this condition, LaPO_4 monomer starts moving from the ‘unique’ facets to other facets due to the internal potential gradient. In this way, a 1D-2D ripening takes place and growth along ‘short axes’ of the nanorods begins. With increase in the autoclaving temperature, the rate of diffusion increases, resulting in enhanced growth along the ‘short axes’ at the cost of growth along the ‘long axis’. Such a preferential growth may be explained as follows: the nature of Lanthanum phosphate monoclinic phase forces growth along the short axis. This means a higher growth rate along the ‘short’ axis and a lower one perpendicular to this axis. The geometric diffusion models proposed independently by Sugimoto, Wey and Karpinski may be invoked here for a lucid description of the preferential growth. As per Yu *et al.*, in the absence of templates, polymers etc., directional growth in crystalline nanomaterials is influenced by a cooperative effect involving thermodynamic preference for directional growth, local solution phenomena, foreign energy activation, and the autogenous pressure.

The photoluminescence spectra of BAM: Eu^{2+} (1.5%) being excited with 254 nm. i.e excitation of the material with 254 nm wavelength generates a broad emission at 470nm. The intensity of peak at 470 nm is relatively very high. As the size of the phosphor reduces the intensity of 470nm peak decreases. By adopting a model where CTS is a combination of $4f^7$ electrons plus a hole, one finds that the resulting spin multiplicities should be 7 and 9. It is the former state that affects optical properties related to the 7F_J state by spin-restricted covalency. The intensity ratio of the luminescence from $^5D_0 \rightarrow ^7F_2$ and from $^5D_0 \rightarrow ^7F_1$ decreases with increasing CTS energy, all of which have the same type of zircon structure. The above intensity ratio is small in $\text{YF}_3:\text{Eu}^{3+}$, even though Eu^{3+} occupies a site without inversion symmetry. It is to be noted that CTSs in fluorides have higher energies than those in oxides. These results suggest that higher CTS energies reduce the strength of the electric dipole transition $^5D_0 \rightarrow ^7F_2$ in Eu^{3+} . The energy of the CTB band depends on the crystal field of the ions surrounding O^{2-} and Eu^{3+} . The red shift in the CTB of nano sized samples implies that the migration of electron density is energetically more facile in these samples than in the bulk sample. This phenomenon clearly indicates that the local environment around O^{2-} and Eu^{3+} ions in nano sized samples is different from that in the bulk one.

The electronic configuration of Eu^{2+} is $4f^7$ and is identical to that of Gd^{3+} . The lowest excited state of 4f levels is located at about $28 \times 10^3 \text{ cm}^{-1}$ and is higher than the $4f^6 5d^1$ level in most crystals, so that Eu^{2+} usually gives broad-band emission due to f-d transitions. The wavelength positions of the emission bands depend very much on hosts, changing from the near-UV to the red. This dependence is interpreted as due to the crystal field splitting of the 5d level, as shown schematically in Figure -3. With increasing crystal field strength, the emission bands shift to longer wavelength. The luminescence peak energy of the 5d-4f transitions of

Eu^{2+} and Ce^{3+} are affected most by crystal parameters denoting electron- electron repulsion; on this basis, a good fit of the energies can be obtained. The near-UV luminescence of Eu^{2+} in $(\text{Sr},\text{Mg})_2\text{P}_2\text{O}_7$ is used for lamps in copying machines using photosensitive diazo dyes. The blue luminescence in $\text{BaMgAl}_{10}\text{O}_{17}$ is used for three-band fluorescent lamps. Red luminescence is observed in Eu^{2+} -activated CaS ; the crystal field is stronger in sulfides than in fluorides and oxides.

The lifetime of the Eu^{2+} luminescence is 10^{-5} – 10^{-6} s, which is relatively long for an allowed transition. This can be explained as follows. The ground state of $4f^7$ is ^8S , and the multiplicity of the excited state $4f^65d^1$ is 6 or 8; the sextet portion of the excited state contributes to the spin-forbidden character of the transition. Sharp-line luminescence at ~ 360 nm due to an f-f transition and having a lifetime of milliseconds is observed when the crystal field is weak so that the lowest excited state of $4f^7(^6\text{P}_J)$ is lower than the $4f^65d^1$ state.

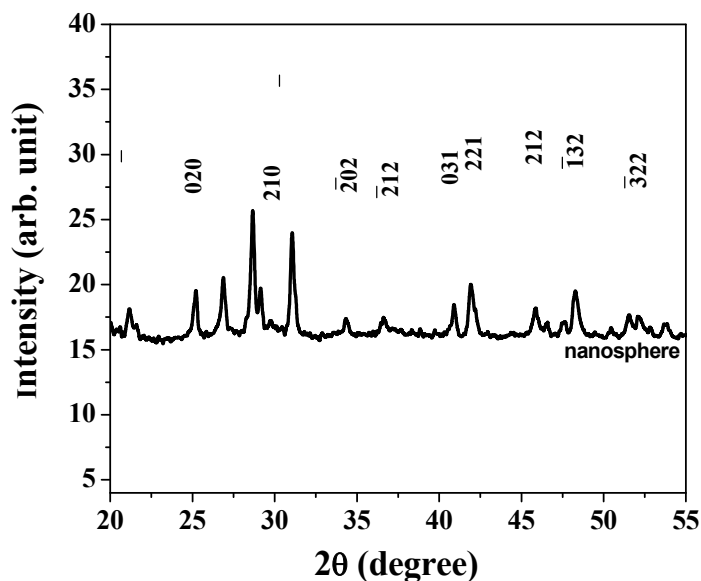


Fig.1: XRD of BAM:Eu

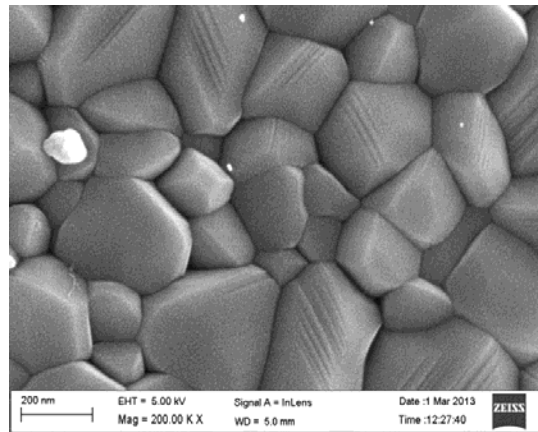


Fig.1: HRSEM of BAM:Eu

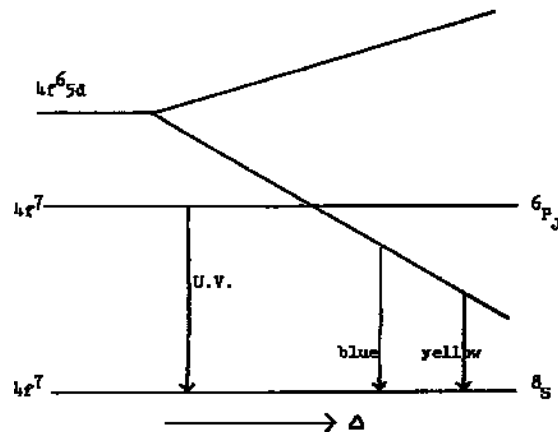


Fig.3: The energies of $4f^7$ and $4f^65d^1$ levels in Eu^{2+} influenced by crystal field

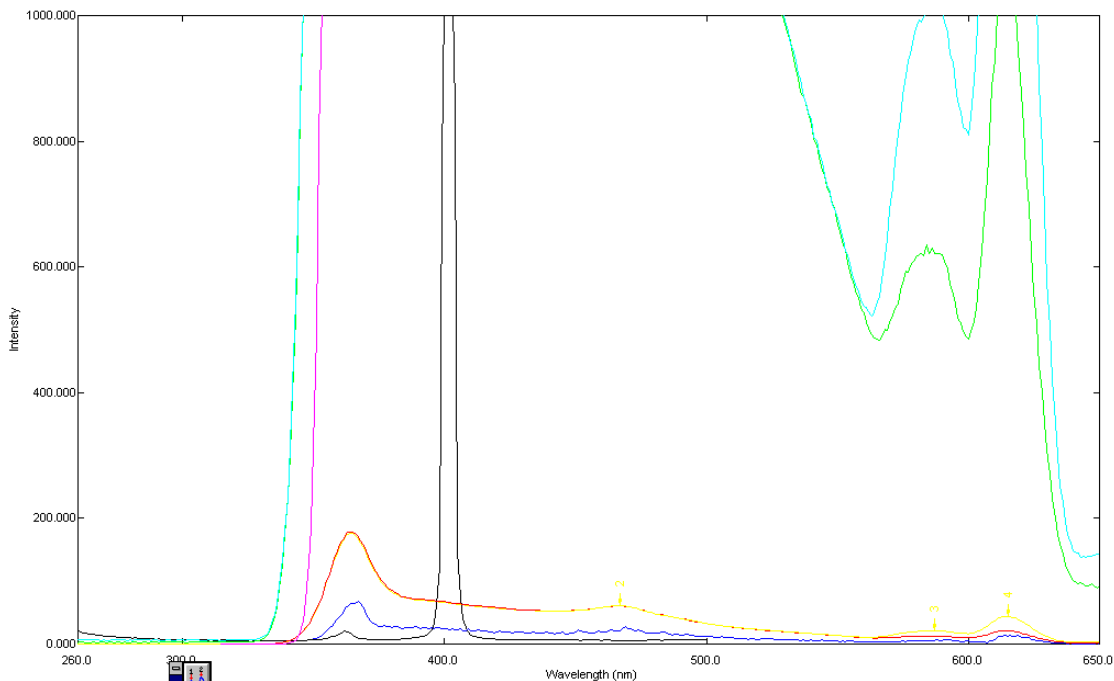


Fig.4: Photoluminescence of BaMgAl₁₀O₁₇-Eu (0.5%),
BaMgAl₁₀O₁₇-Eu (1.0%), BaMgAl₁₀O₁₇-Eu (1.5%)

Conclusion: The main PL emission is around 470nm which is due to allowed transitions of Eu²⁺ in BAM and also other peaks of Eu 590 and 615nm were found. As the size of the phosphor reduces from micro to nano the intensity of 470nm peak decreases. This confirms the formation of nano phosphor due to high intensity and long duration ball milling.

Acknowledgement: One of the author ASP is thankful to UGC MRP project NO:MRP-6176/15(UGC-SER0) dated Jan,2015.

References:

1. Hoshina, T., Imanaga, S., and Yokono, S., *J. Luminesc.*, 15, 455, 1977.
2. Blasse, G., *Material science of the luminescence of inorganic solids*, in *Luminescence of Inorganic Solids*, DiBartolo, B., Ed., Plenum Press, 1978, 457.
3. Smets, B.M.J. and Verlijdsdonk, J.G., *Mater. Res. Bull.*, 21, 1305, 1986.
4. Takahashi, K., Kohda, K., Miyahara, J., Kanemitsu, Y., Amitani, K., and Shionoya, S. *J. Luminesc.*, 31&32, 266, 1984.
5. Hews, R.A. and Hoffman, M.V., *J. Luminesc.*, 3, 261, 1970.
6. Ryan, F.M., Lehmann, W., Feldman, D.W., and Murphy, J., *J. Electrochem. Soc.*, 121, 1475, 1974.
7. Z. A. Peng, X. Peng, *J. Am. Chem. Soc.*, 123 (2001) 1389–1395.



8. Nanostructures & nanomaterials: synthesis, properties & applications Guozhong Cao, Imperial College Press, Pg. 127-130 London, 2004.
9. T. Sugimoto, J. Imaging Sci., 33 (1989) 203–205.
10. P. S. Karpinski, J. H. Wey, J. Imaging Sci., 32 (1988) 34–39.
11. S. H. Yu, B. Liu, M. S. Mo, J. H. Huang, X. M. Liu, Y.T. Qiu, Adv. Func. Mater. 13 (2003), 639–647.
12. P. Ghosh, A. Patra, J. Nanosci. Nanotech. 8 (2008) 3458–3464.